

Article

# Impact of North Atlantic Teleconnection Patterns on Northern European Sea Level

Léon Chafik <sup>1,\*</sup>,<sup>†</sup> , Jan Even Øie Nilsen <sup>2</sup>  and Sönke Dangendorf <sup>3</sup>

<sup>1</sup> Geophysical Institute, University of Bergen, and Bjerknes Centre for Climate Research, 5020 Bergen, Norway

<sup>2</sup> Nansen Environmental and Remote Sensing Center, and Bjerknes Centre for Climate Research, 5006 Bergen, Norway; jan.even.nilsen@nersc.no

<sup>3</sup> Research Institute for Water and Environment, University of Siegen, 57076 Siegen, Germany; Soenke.Dangendorf@uni-siegen.de

\* Correspondence: leon.chafik@uib.no; Tel.: +47-55-20-58-00

† Current address: Universitetet i Bergen, Geofysisk institutt, Postboks 7803, 5020 Bergen, Norway.

Received: 31 May 2017; Accepted: 30 August 2017; Published: 6 September 2017

**Abstract:** Northern European sea levels show a non-stationary link to the North Atlantic Oscillation (NAO). The location of the centers of the NAO dipole, however, can be affected through the interplay with the East Atlantic (EAP) and the Scandinavian (SCAN) teleconnection patterns. Our results indicate the importance of accounting for the binary combination of the NAO with the EAP/SCAN for better understanding the non-stationary drivers inducing sea level variations along the European coasts. By combining altimetry and tide gauges, we find that anomalously high monthly sea levels along the Norwegian (North Sea) coast are predominantly governed by same positive phase NAO+/EAP+ (NAO+/SCAN+) type of atmospheric circulation, while the Newlyn and Brest tide gauges respond markedly to the opposite phase NAO−/EAP+ combination. Despite these regional differences, we find that coherent European sea level changes project onto a pattern resembling NAO+/SCAN+, which is signified by pressure anomalies over Scandinavia and southern Europe forcing winds to trace the continental slope, resulting in a pile-up of water along the European coasts through Ekman transport. We conclude that taking into consideration the interaction between these atmospheric circulation regimes is valuable and may help to understand the time-varying relationship between the NAO and European mean sea level.

**Keywords:** European sea level; atmospheric circulation; teleconnections; satellite altimetry; tide gauges

## 1. Introduction

Global mean sea level has been accelerating from rates of 1.1 to 2 mm/year before 1990 [1] towards unprecedented high rates of  $3.3 \pm 0.4$  mm/year afterwards [2] and is expected to continue its acceleration in a warming climate primarily as a result of melting ice and ocean thermal expansion [3,4] giving rise to significant socioeconomic and environmental consequences on the coastal zones [5]. Rising seas can, however, deviate immensely on regional scale relative to the global mean owing to several processes acting at different locations on a range of timescales [6–8].

Wind forcing over the North Atlantic, for instance, can cause regional and coastal mean sea level variations acting from months to decades [9–11]. However, since the North Atlantic meridional dipole of the mean sea level pressure field is subject to spatial displacements (non-stationarity), the relationship between northern European sea level and atmospheric forcing, as typically defined by the North Atlantic Oscillation, is found to be temporally variable (e.g., Wakelin et al. [12]). This non-stationarity of the centers of action is presumed to induce notable impacts on northern European sea level (e.g., Dangendorf et al. [13]). The present study therefore focuses on understanding

the response of northern European sea level to this non-stationarity of the centers of action through a simple approach that combines the three prominent North Atlantic teleconnection patterns [14].

Strong and weak periods of atmospheric forcing in the North Atlantic region are usually linked to the strength of the prevailing westerly winds as measured by the meridional mean sea-level pressure (MSLP) gradient between the Icelandic low and the Azores high, i.e., the North Atlantic Oscillation (NAO); a major mode of North Atlantic climate and ocean circulation variability [15–18]. During its positive phase, the westerlies are anomalously strong and more intense storms are generated. While during a negative NAO phase, the winds are weaker than normal and the jet stream and hence the storm tracks are shifted southward [15]. However, several recent studies have indicated that the NAO index alone is not sufficient to explain the climatic variations over both ocean [19,20] and land [21–24], and that other teleconnections, typically the second and third leading mode of atmospheric variability in the North Atlantic/European sector [25–27], are important to take into consideration. The reasoning is that North Atlantic climate variability is influenced by spatial movements of the centers of action that can only be captured when combining the NAO with the other two leading modes [14,28]. Already in 1939, Rossby [29] recognized that displacements of the semi-permanent centers of action are able to influence the climate system. Woollings et al. [30], for example, showed that the latitudinal position of the eddy-driven jetstream can be explained by a combination of the NAO and the East-Atlantic Pattern (EAP, the second leading mode). The latter was recently suggested by Comas-Bru and McDermott [23] to influence temperature and precipitation patterns over Europe, often also together with the Scandinavian pattern (SCAN, the third leading mode [27]).

From a sea-level perspective, a number of studies have reported on the impact of the NAO on the mean sea level, its variability, sensitivity and related processes [12,31–39]. Yan et al. [33] and Jevrejeva et al. [34] find that the NAO co-varies strongly with the sea level in northwest Europe using tide gauges dating back to the 19th century, but they also point out that this relationship is not stable over time. In particular, it was strongly enhanced during the second half of the 20th century. This finding is in agreement with that of Wakelin et al. [12], where the 1909–1954 period was reported to exhibit lower correlations with the NAO from 17 tide gauges in the North Sea region as compared to higher correlations during the 1955–2000 period (see also Andersson [31]). But although this intermittency in the relationship of the sea level to the NAO is argued to have been induced by shifts in the centers of action (see, e.g., Hilmer and Jung [40], Jung et al. [41]), the influence of this non-stationarity of the atmospheric circulation on the sea level along the European coasts remains poorly quantified. Perhaps with the exception of the studies by Kolker and Hameed [42] and Ullmann and Monbaliu [43]. The former assessed the influence of shifts in the position of the centers of action on sea level change at five tide gauges in the Atlantic, while the latter focused on daily sea surges at a single station along the Belgian coast and their relationship to weather regimes.

In this study, we utilize satellite altimetry, tide gauges and atmospheric reanalysis to investigate the influence of the migrations of the North Atlantic meridional pressure dipole on the sea level along the European shelves and coasts through the combination of the canonical NAO, EAP and SCAN patterns. Our findings suggest that the NAO alone is not always sufficient as a forcing mechanism (see, e.g., Dangendorf et al. [13], Kolker and Hameed [42], Ullmann and Monbaliu [43]), and that it is essential to take into account all three leading modes of North Atlantic atmospheric variability to explain the anomalous periods of the European sea level, not least since there are regional differences with a preference toward a specific atmospheric pattern that can only be formed by the linear combination of these teleconnections [14].

The paper is structured as follows. Section 2 describes the data and methodology. Section 3 shows the North Atlantic teleconnection patterns, their linear combinations, and how they influence the sea level along the European shelves and coasts consistently using both altimetry and tide gauges. These results are followed by a summarizing discussion and outlook in Section 4.

## 2. Data and Methodology

### 2.1. Satellite Altimetry

We use the DUACS DT2014 multi-mission satellite altimetry [44] to study the sea-level variability on the European continental shelf, Figure 1. An important change in the DT2014 is the referencing of the sea level anomaly products to the 20 years of available measurements as compared to the previous 7-year reference period. The new reprocessed sea level anomaly products demonstrate multiple significant improvements in, e.g., mesoscale signals, eddy kinetic energy, geostrophic currents (now more comparable to surface drifter observations) and sea level at higher latitudes as well as in coastal areas [44]. The DT2014 demonstrates a better consistency with sea levels from tide gauge stations. The geophysical corrections pertaining to inverse barometer, tides and dry/wet tropospheric effects have been applied beforehand. We here utilize the monthly mean absolute dynamic topography (the sum of sea-level anomalies and the MDT\_CNES/CLS 2013 ocean mean dynamic topography) averaged from daily data, on a  $1/4^\circ$  cartesian grid, between January 1993 and December 2015.

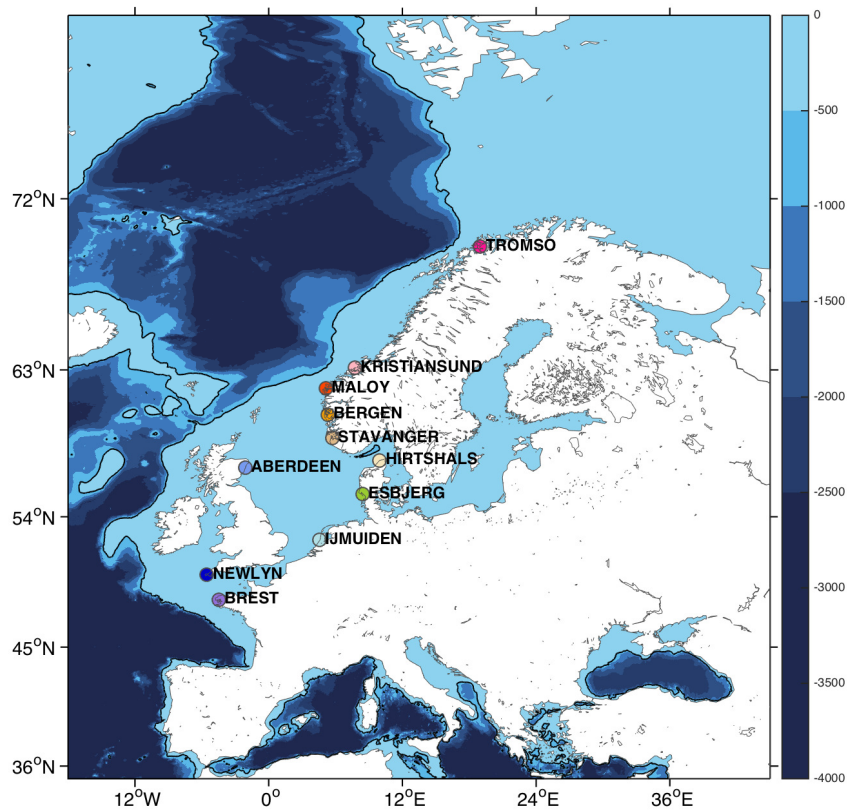


**Figure 1.** Bathymetric map (m) including the location of the 11 tide gauges used in this study. The 500 m isobath is indicated in black.

### 2.2. Tide Gauges

Monthly data from 11 tide gauges (TGs) along the European coasts are used, Figure 1. This data was downloaded from the webpage of the Permanent Service for Mean Sea Level (PSMSL) [45], and have been corrected for the inverse barometer effect using the National Center for Environmental Prediction/National Center for Atmospheric Research (NCEP/NCAR) reanalysis [46], linearly detrended, and deseasonalized by removing the mean seasonal cycle. The TG period under investigation stretches from January 1950 until December 2014. Note, however, that although a

weak relationship during the 1909–1954 period between sea levels from tide gauges and the NAO has been reported (e.g., Wakelin et al. [12]), using these data since 1950 is not an issue for our results.

### 2.3. Atmospheric Data

We use the monthly NCEP/NCAR reanalysis [46] monthly mean sea level pressure (MSLP) and winds at 10 m spanning the 1950–2015 period. The grid resolution of this data is  $2.5^\circ \times 2.5^\circ$ . The monthly data have been linearly detrended, and deseasonalized by removing the mean seasonal cycle. The MSLP is used to calculate the three leading empirical orthogonal functions (EOFs) of atmospheric variability in the North Atlantic/European sector ( $80^\circ\text{W}$ – $50^\circ\text{E}$ ,  $30^\circ\text{N}$ – $80^\circ\text{N}$ ) following the method described by Hannachi et al. [47], which is based on singular value decomposition. The data are weighted by the cosine of its latitude at every grid point.

### 2.4. Linear Combination of the Leading EOFs

The three leading EOFs together explain more than 60% of the monthly atmospheric variability in the North Atlantic/European sector. During wintertime, they explain, however, more than 90% of the variability in the subpolar North Atlantic and northern Europe [14]. The reasoning behind the linear combination is that although the north-south meridional MSLP dipole associated with the NAO is the dominant pattern, the atmospheric circulation, at any given time, is not solely composed of a pure NAO phase but rather involves the other two leading teleconnections, i.e., the East Atlantic Pattern (EAP) and Scandinavian Pattern (SCAN), which result in horizontal displacements of the centers of action. The linear combination of MSLP can thus be written, following [14], as:

$$MSLP = \alpha \times NAO + \beta \times \left\{ \begin{matrix} EAP \\ SCAN \end{matrix} \right\}$$

where  $\left\{ \begin{matrix} \alpha \\ \beta \end{matrix} \right\} = [-1, 0, 1]$

The two phases of the NAO (EAP/SCAN) occur when  $\alpha = \pm 1$  ( $\alpha = 0$ ) and  $\beta = 0$  ( $\beta = \pm 1$ ), while the other four possible linear combinations occur when  $\alpha$  and  $\beta$  are  $\neq 0$ . Moore et al. [14] show that this simple technique is able to capture the fundamental characteristics associated with the mobility of the centers of action; atmospheric variability is not a result of a single EOF, but instead results from a continuum of EOFs that are acting simultaneously, and can thus be reconstructed by the linear combination of these climate modes [28].

## 3. Results

### 3.1. North Atlantic Teleconnections and Their Interaction

The three leading modes of atmospheric variability in the North Atlantic/European sector are the NAO, EAP and SCAN. These three EOFs explain 32%, 17% and 15% of the MSLP variability over the 1950–2015 period based on the NCEP/NCAR reanalysis, Figure 2. The North Atlantic meridional MSLP dipole, i.e., between the region near Iceland/western Nordic Seas and the Azores, is a distinctive pattern of the first leading EOF, i.e., the NAO. The second leading EOF, i.e., the EAP, is primarily characterized by a monopole pressure encompassing the subpolar North Atlantic region with a node south of Iceland. The third EOF, i.e., the SCAN, is centered over the southern parts of Norway with a node close to Bergen (cf. Figure 1). Note, however, that the EAP and SCAN have another node over Eastern Europe and Greenland, respectively, albeit rather weak. It should also be mentioned that the EAP and SCAN are associated with the known weather regimes Atlantic ridge and Scandinavian blocking, respectively (see Cassou et al. [48]).

We now look into the atmospheric patterns when the NAO is linearly combined with the EAP (Figure 3) and SCAN (Figure 4). Figure 3 shows that during same (opposite) sign NAO-EAP events, the centers of action shift southwestward (northeastward). Due to these displacements, the zero line

during, e.g., NAO+/EAP+ (NAO+/EAP−) conditions follows the North European coast (becomes more zonally-oriented).

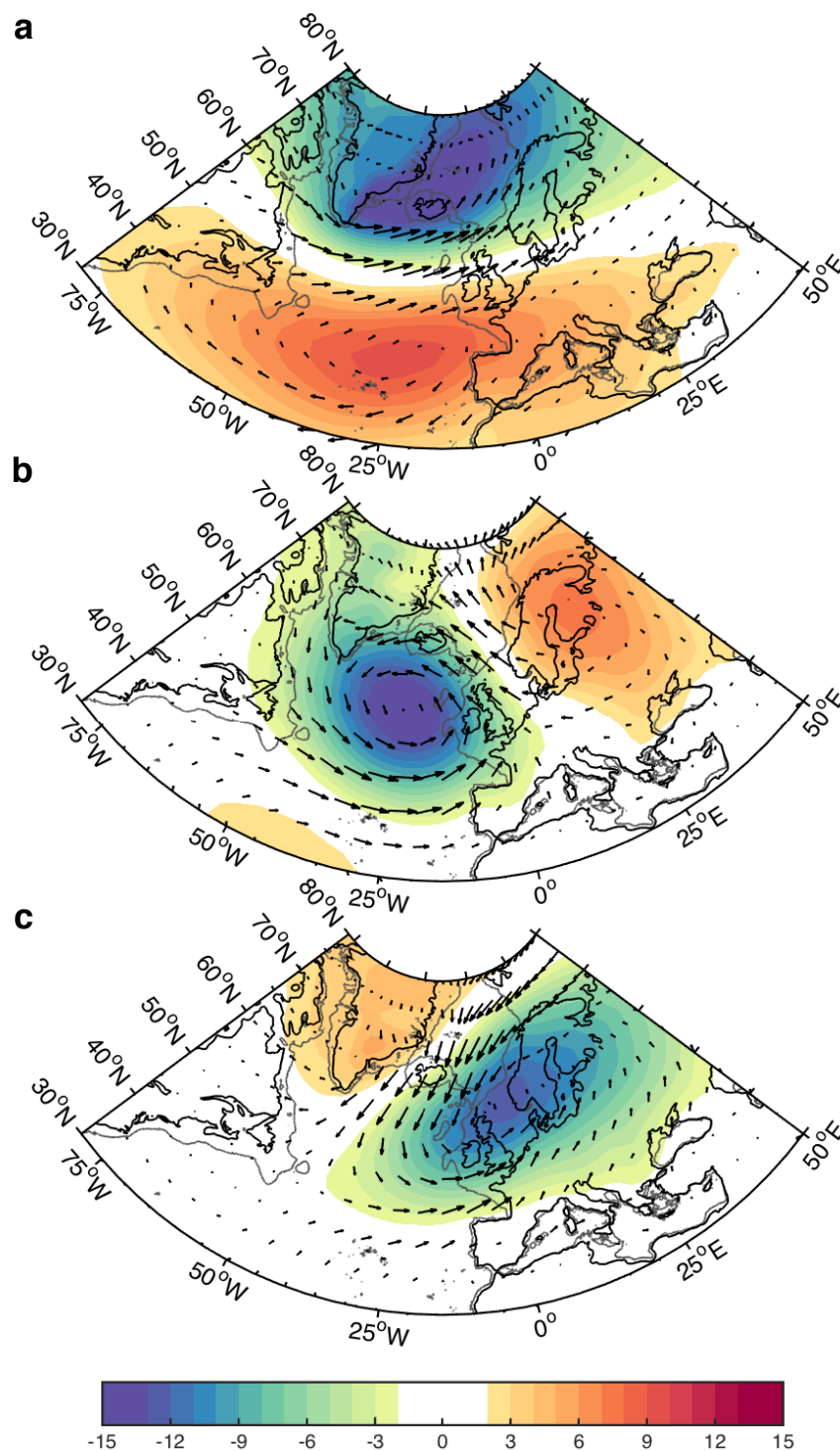


**Figure 2.** Composite analysis of MSLP (hPa) and 10 m winds based on the (a) NAO, (b) EAP and (c) SCAN teleconnection indices calculated using NCAR/NCEP for the 1950–2015 period. The composite difference is based on anomalously high ( $>0.75$  std) and low ( $<-0.75$  std) periods of the three leading principal components of MSLP.

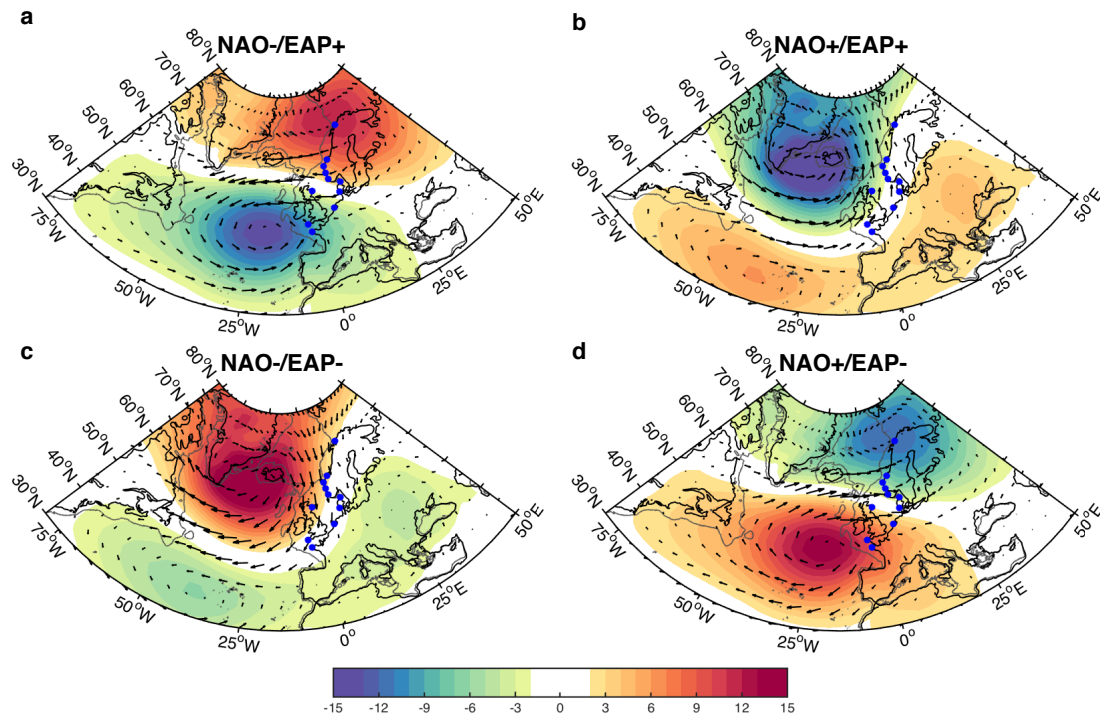


**Figure 3.** Meridional mean sea-level pressure (hPa, shading) and 10 m wind (vectors) patterns based on the four linear NAO-EAP combinations. (a) Negative and (b) positive NAO combined with the positive phase of the EAP. (c) Negative and (d) positive NAO combined with the negative phase of the EAP. The TG stations are overlaid to help with the orientation.

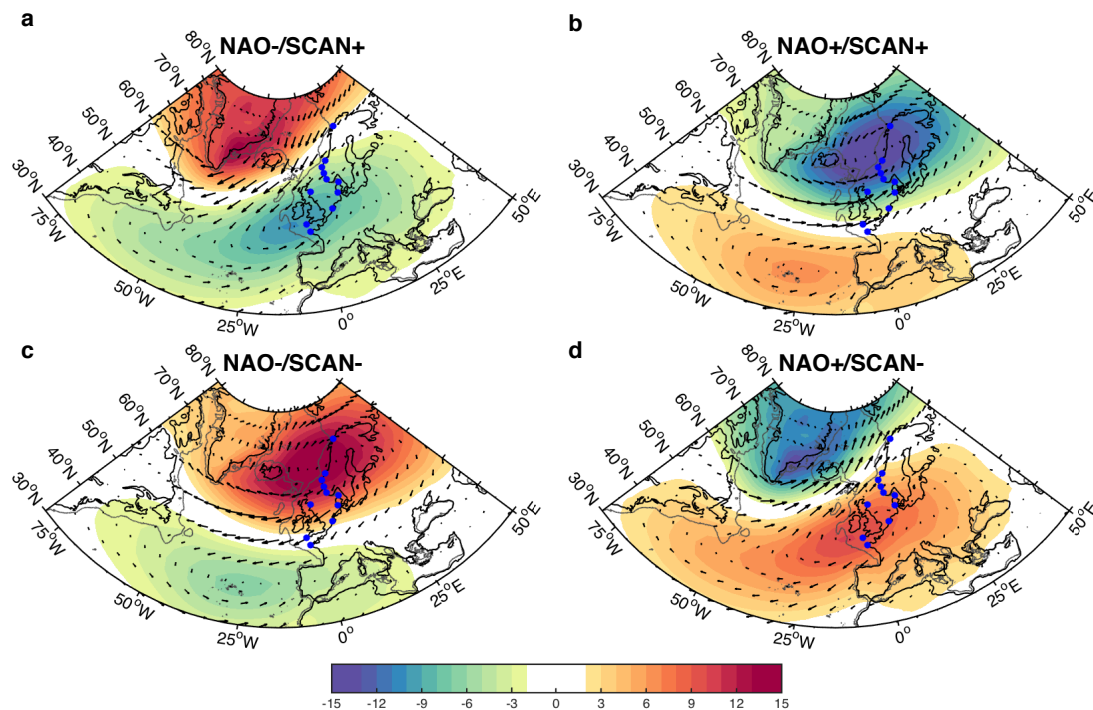


**Figure 4.** Meridional mean sea-level pressure (hPa, shading) and 10 m wind (vectors) patterns based on the four linear NAO-SCAN combinations. (a) Negative and (b) positive NAO combined with the positive phase of the SCAN. (c) Negative and (d) positive NAO combined with the negative phase of the SCAN. The TG stations are overlaid to aid with the orientation.

During same sign NAO-SCAN conditions (Figure 4), the northern node moves to the east over the Norwegian Sea, and the southern one moves to the west (and slightly to the south), now being more localized over the Azores. While during opposite sign NAO-SCAN events the northern anomaly is more displaced to the west over eastern Greenland, and the southern anomaly migrates northwards and to the east with a node just south off the British Isles resulting in an overall slanted spatial pattern. In general, the interplay between the NAO and the SCAN induces clockwise (anticlockwise) movements of the centers of action when having the same (opposite) sign. The impact of the NAO-EAP combination on the winter MSLP field reported by Moore et al. [14] are similar to our results shown in Figures 3 and 4.

### 3.2. The Combined Impact on European Sea Level as Seen in Altimetry

Before diagnosing the impact of the combined EOFs on the sea level along the European shelves and coasts, we show in Figure 5 how the sea level responds to the three leading teleconnection patterns separately. Figure 5a shows a coherent positive relationship to sea level over both the Norwegian and North Seas as a response to the NAO and its associated winds flowing parallel to these coasts (Figure 2a). Note that the magnitudes are larger along the coasts with the highest sea levels over the German Bight and the Baltic Sea (>0.15 m) [31]. The sea-level response to the EAP is dominated by a dipole pattern between the sea level in the North/Baltic Sea and elsewhere on the European shelves (Figure 5b). The negative and weakly positive sea level anomalies in the North Sea and Norwegian Sea, respectively, is mainly due to the large-scale winds being offshore-directed as a result of the EAP monopole structure over the subpolar North Atlantic region (Figure 2b). The response to positive SCAN periods is anomalously low sea level in the interior of the North Sea, along the Norwegian coast and the Barents Sea, and anomalously high sea level along a narrow coastal zone stretching from the Bay of Biscay to the northern tip of Denmark close to the Hirtshals TG station, as well as in the Baltic Sea (Figure 5c). Anomalously low MSLP in the outer part of the North Sea associated with the SCAN (cf. Figure 2c) induces alongshore winds in the inner part that ultimately lead to this sea level pattern.

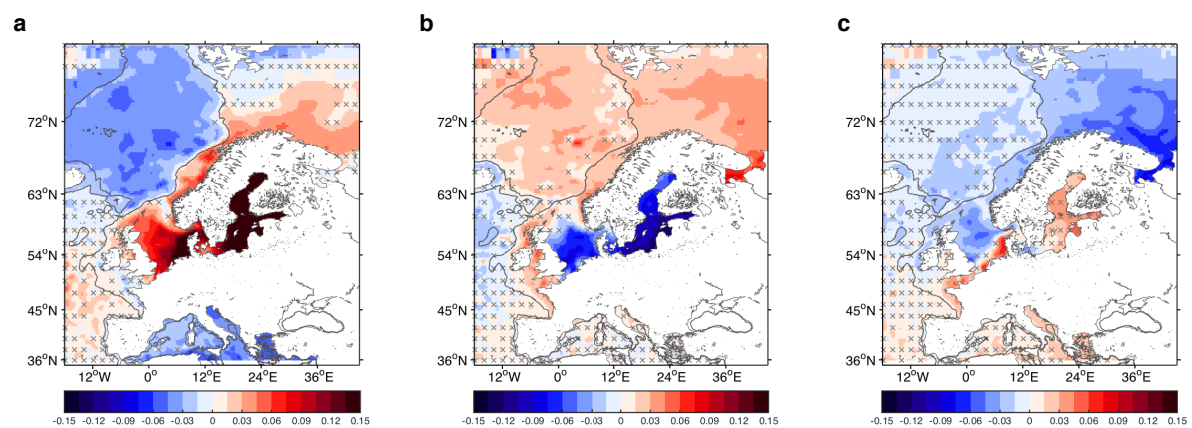


**Figure 5.** Sea level composite difference (m) from altimetry during the 1993–2015 period based on the (a) NAO, (b) EAP and (c) SCAN indices. The threshold value for the composites is 0.75 std of the teleconnection indices. The non-significant regions are indicated by gray crosses calculated using a two-sided *t* test.

We diagnose the effect of the binary interaction between the NAO with the EAP (Figure 6) and SCAN (Figure 7) on the sea level during the altimetry period, i.e., 1993–2015. The same and opposite phase combinations are observed to affect the northern shelf seas differently. Events with NAO-EAP values of the same sign show a more coherent spatial sea level pattern along the Norwegian shelf and the Barents Sea. There is little (only weak and regionalized as for the EAP alone) influence on the North Sea associated with same sign NAO-EAP events. In contrast, NAO-EAP values of the opposite

sign show a strong influence on the sea level in the North and Baltic Seas. The phases of the EAP thus have different impacts on the North Sea and the Norwegian Sea, which can be attributed to the displacements of the centers of action and the orientation of the large-scale wind field. In the case of same sign NAO-EAP events, the winds closely trace the Norwegian coast (cf. Figure 3b,c) ultimately leading to anomalous (higher for NAO+/EAP+ situations) sea levels on the shelf, Figure 6b,c. While, during opposite sign situations, the modulation of the meridional pressure gradient enhances the westerlies across the North Sea (Figure 3a,d; note that the zero line crosses the North Sea), which plays an important role for the observed sea-level pattern in Figure 6a,d. These results are consistent with the findings of Dangendorf et al. [11], where anomalous sea-level situations between 1871 and 2011 from 14 tide gauges (located along the coasts of Belgium, Netherlands, Germany and Denmark, see their Figure 1 and regions 1–2) are shown to be strongly influenced by this westerly flow due to a low-pressure anomaly located over northern Scandinavia, which resembles the position of the northern center of action reflected by opposite sign NAO-EAP events.

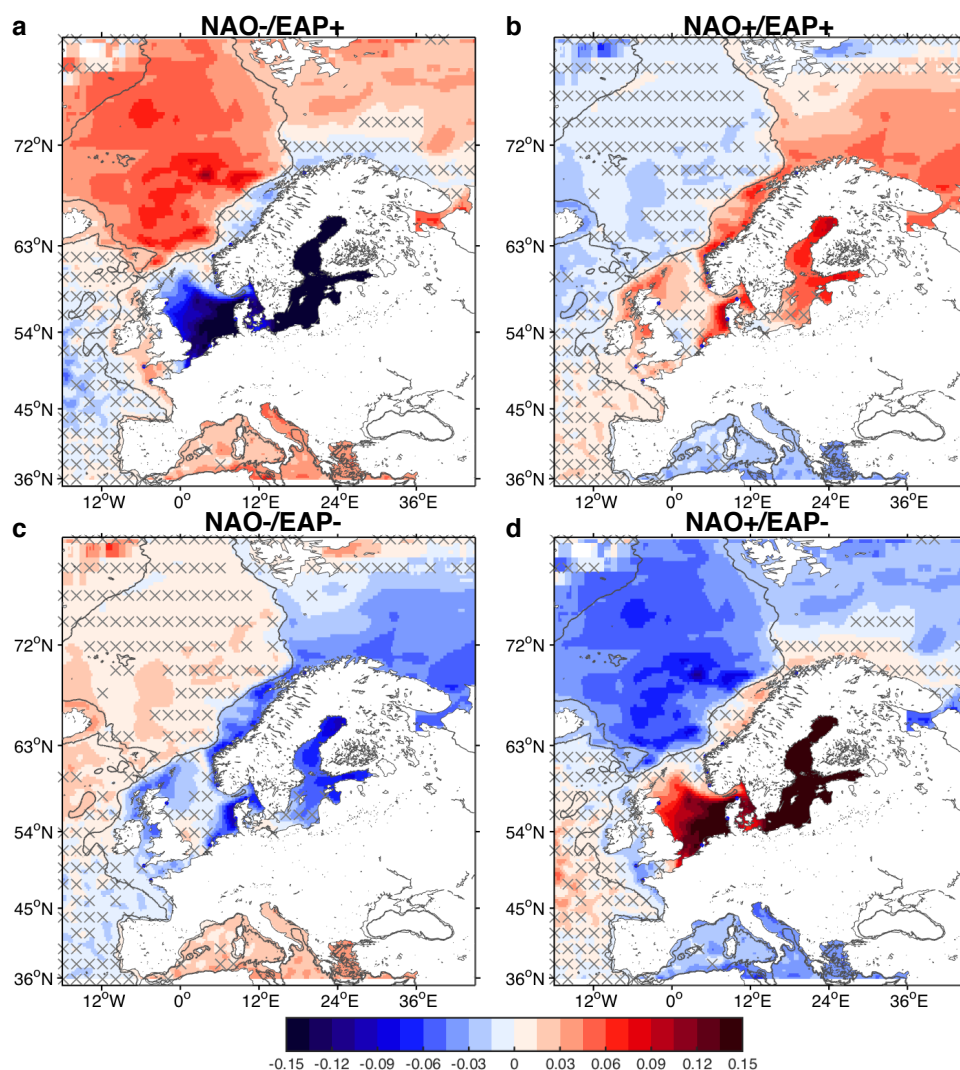


**Figure 6.** Sea level composite difference (m) from altimetry during the 1993–2015 period based on the four linear combinations of the NAO with the EAP. (a) Negative and (b) positive NAO combined with the positive phase of the EAP. (c) Negative and (d) positive NAO combined with the negative phase of the EAP. The threshold value for the composites is 0.75 std. The TG stations are overlaid to aid with the orientation. The non-significant regions below the 95% confidence level are indicated by gray crosses calculated using a two-sided *t* test.

The maximum (minimum) sea level associated with same sign NAO+/SCAN+ (NAO−/SCAN−) events appears to be locally concentrated to the German Bight and the Baltic Sea, cf. Figure 7. However, the opposite phases of the NAO-SCAN show a coherent sea level pattern dominating the North and Norwegian Seas, which is an immediate response to the anticlockwise movement and the slanting behavior of the centers of action ultimately reorganizing the wind field to be parallel to these coasts (Figure 4a,d).

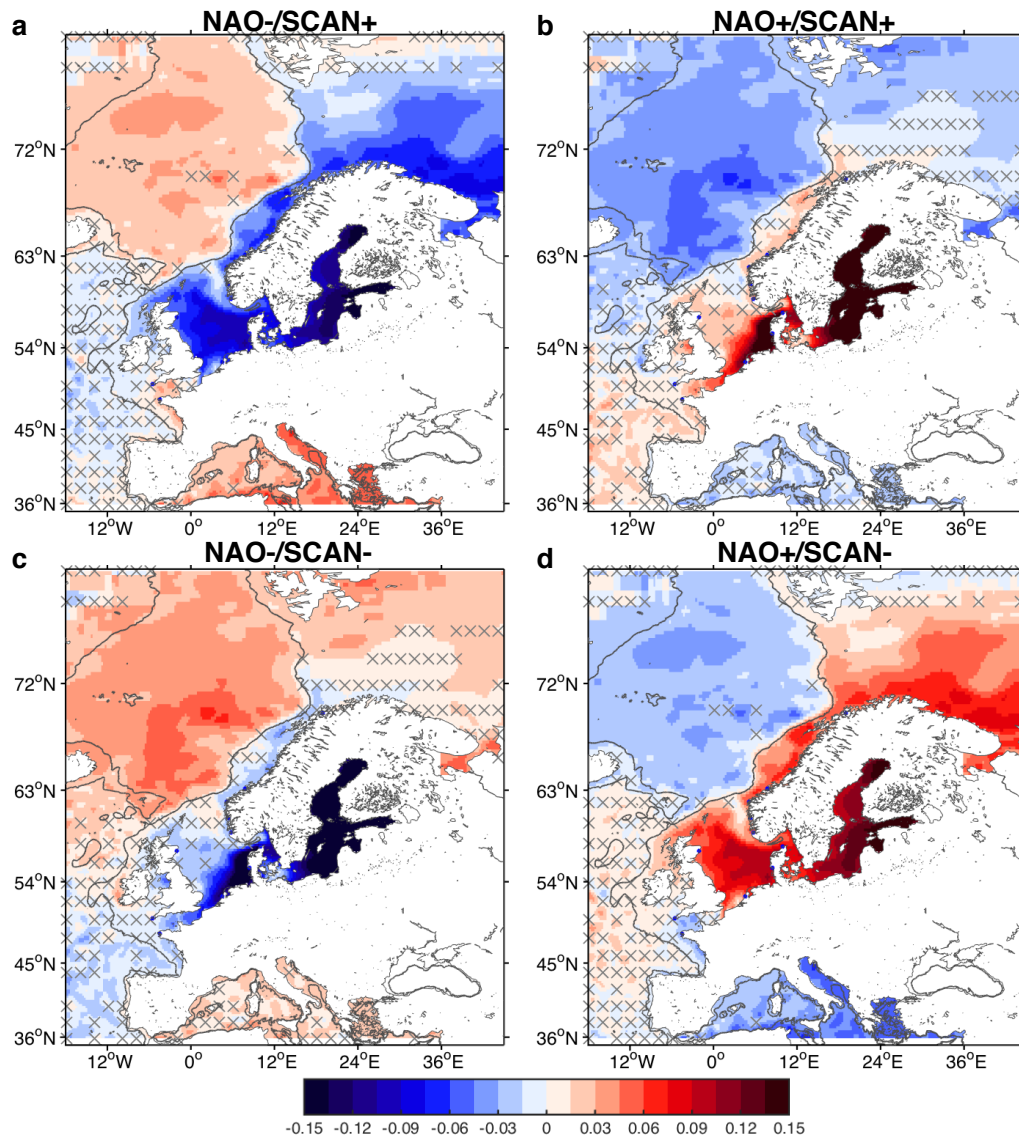


**Figure 7.** Sea level composite difference (m) from altimetry during the 1993–2015 period based on the four linear combinations of the NAO with the SCAN. (a) Negative and (b) positive NAO combined with the positive phase of the SCAN. (c) Negative and (d) positive NAO combined with the negative phase of the SCAN. The threshold value for the composites is 0.75 std. The TG stations are overlaid to aid with the orientation. The non-significant regions below the 95% confidence level are indicated by gray crosses calculated using a two-sided *t* test.

### 3.3. The Combined Impact on the European Coasts as Seen in Tide Gauges

We have shown in the previous section that anomalous periods of the teleconnection patterns and their interaction induce regional sea-level differences along the European shelves and coasts as observed during the altimetry period (1993–2015). We now investigate whether these regional

differences are also present in TG records during the 1950–2014 period at the 11 European stations shown in Figure 1. We find that the sea level response at these tide gauges mirror to great detail the regional sea level structures manifested in altimetry and related to the combined effects of the NAO and either the EAP or SCAN (Figure 8).

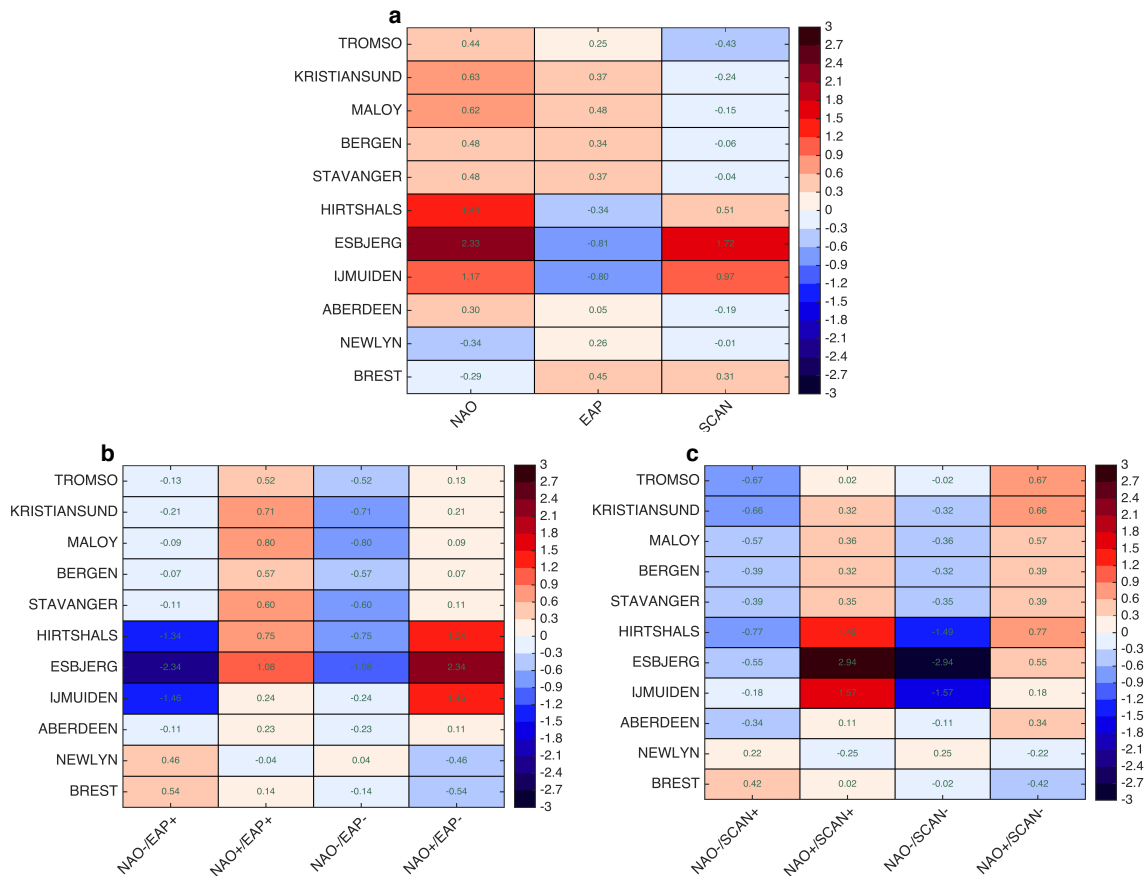


**Figure 8.** Composite difference of sea level (m) from the TGs based on the (a) three leading principal components of MSLP separately, (b) NAO-EAP and (c) NAO-SCAN combinations.

At the Norwegian TGs (Tromsø–Stavanger), the sea-level response is stronger during periods of same sign NAO-EAP combination as compared to those induced by the NAO or the EAP only (Figure 8a,b). For Brest and Newlyn, opposite sign NAO-EAP events appear to result in more anomalous sea levels as compared to any other mode or sign combination. Concerning the North Sea tide gauges, the NAO-EAP combinations (either same or opposite sign) do not show any more influence on the sea level than the NAO alone. However, events of same sign NAO-SCAN combinations are very likely to induce significantly stronger sea-level anomalies than solely through the NAO, especially for Esbjerg and Ijmuiden stations.

### 3.4. Teleconnection Space and Anomalous Sea Level at the European Coasts

Another approach to illustrate the preferred atmospheric state leading to anomalous sea-level periods at each TG station is to project these onto a space spanned by the NAO and the EAP (Figure 9) or SCAN (Figure 10) indices. Doing so, we study the spatial behavior and count how many of these anomalous months actually fall in the different quadrants spanned by the teleconnection indices. We can thus generalize the preferred combinations driving anomalous (>0.75 std) as well as extreme (>1.5 std) monthly sea levels as recorded at the TG stations along the European coasts.

Figure 9 demonstrates that both anomalously and extremely high monthly sea levels recorded from tide gauges along the Norwegian coast (Stavanger, Bergen, Måløy, Kristiansund and Tromsø) are dominated by the NAO+/EAP+ type of pattern, i.e., the corresponding same sign NAO-EAP values are clustered towards the upper-right quadrant. On average, about 45% (54%) of the anomalously (extremely) high monthly sea levels, respectively, are found in this quadrant. Anomalously high monthly sea levels recorded at tide gauge stations in the North Sea (Ijmuiden, Esbjerg, Hirtshals) are strongly dominated by NAO+/EAP-. On average, about 51% (59%) of the anomalous (extreme) monthly sea levels are clustered in the NAO+/EAP- quadrant. The tide gauges located in the south, i.e., Newlyn and Brest are also dominated by opposite sign NAO-EAP values, however, NAO-/EAP+ conditions are more likely to induce anomalously (extremely) high monthly sea levels, with an average of 46% (54%) of these months being clustered in this quadrant. As shown in Figure 3a, the NAO-/EAP+ pattern is characterized by a low-pressure anomaly outside the Bay of Biscay, which induces cyclonic winds parallel to the continental slope resulting in coastal convergence and anomalously high sea level.

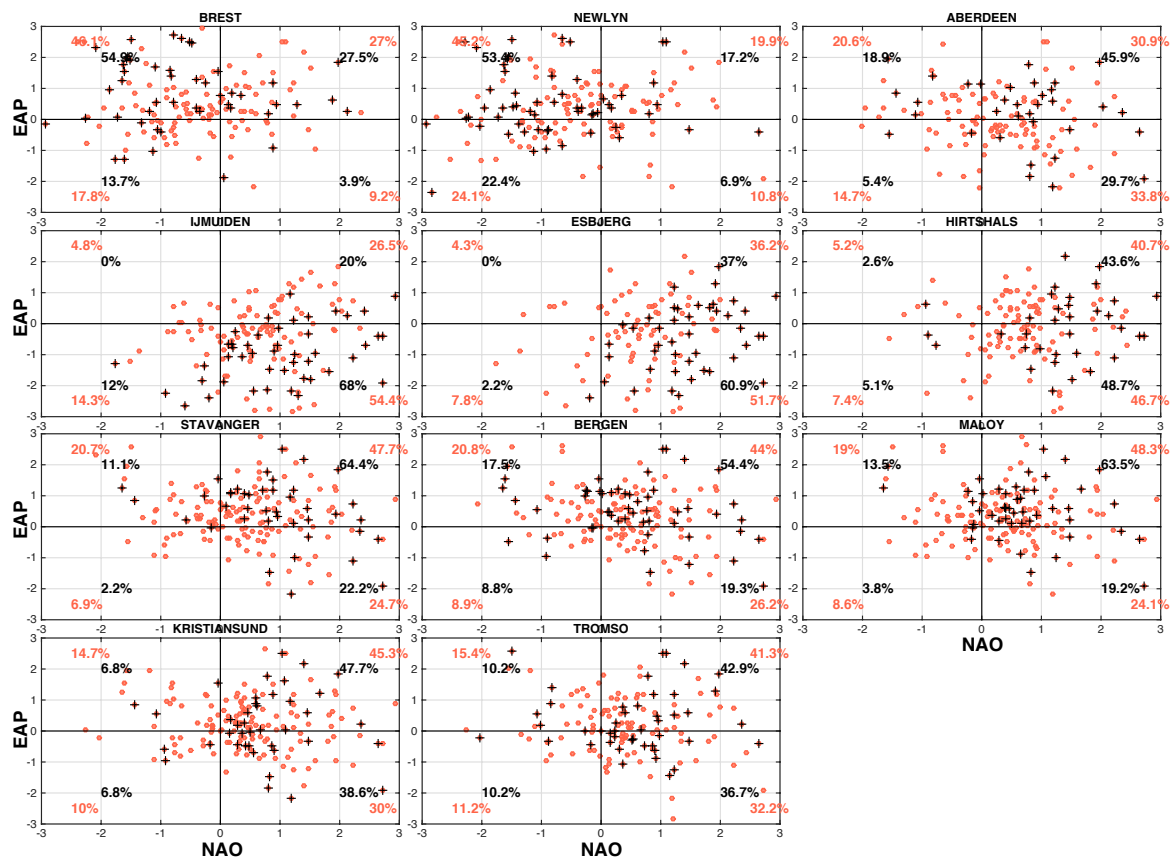


**Figure 9.** Anomalously/extremely high (red circles/black crosses) monthly sea levels recorded at the different TGs along the European coasts projected onto the NAO-EAP teleconnection space. The threshold value for the anomalous/extreme monthly sea levels is 0.75/1.5 std. The percentages represent the number of anomalously/extremely high (in red/black) months in every quadrant divided by the total number of anomalously high/extreme months in all quadrants.

Figure 10 underlines that opposite sign NAO-SCAN events are more likely to induce anomalous (extreme) monthly sea levels along the Norwegian coast (but also Aberdeen), with an average of 42% (48%) of these months being clustered in the NAO+/SCAN- quadrant. A notable feature, however, is that this relationship becomes more distinct as a function of latitude. For example, the number of anomalously (extremely) high monthly sea levels recorded at Tromsø and clustered

in the NAO+/SCAN− quadrant is 51% (59.2%) compared to 36.3% (38.6%) in Bergen. A possible explanation is that since the NAO+/SCAN− leads to anticlockwise movements of the centers of action, the winds are thus better aligned with the continental slope in the northern parts of Norway (cf. Figure 4). The anomalously (extremely) high monthly sea levels observed at the North Sea tide gauges, however, are strongly dominated by NAO+/SCAN+, i.e., same sign values. Ijmuiden, Esbjerg and Hirtshals have 57.8% (68%), 65.5% (80.4%) and 51.9% (59%) of their anomalously (extremely) high monthly sea levels in the NAO+/SCAN+ quadrant. These high numbers are not surprising considering the strong cyclonic wind anomalies over the northern Seas induced as a result of the clockwise movement and intensification of the low-pressure node (cf. Figure 4).

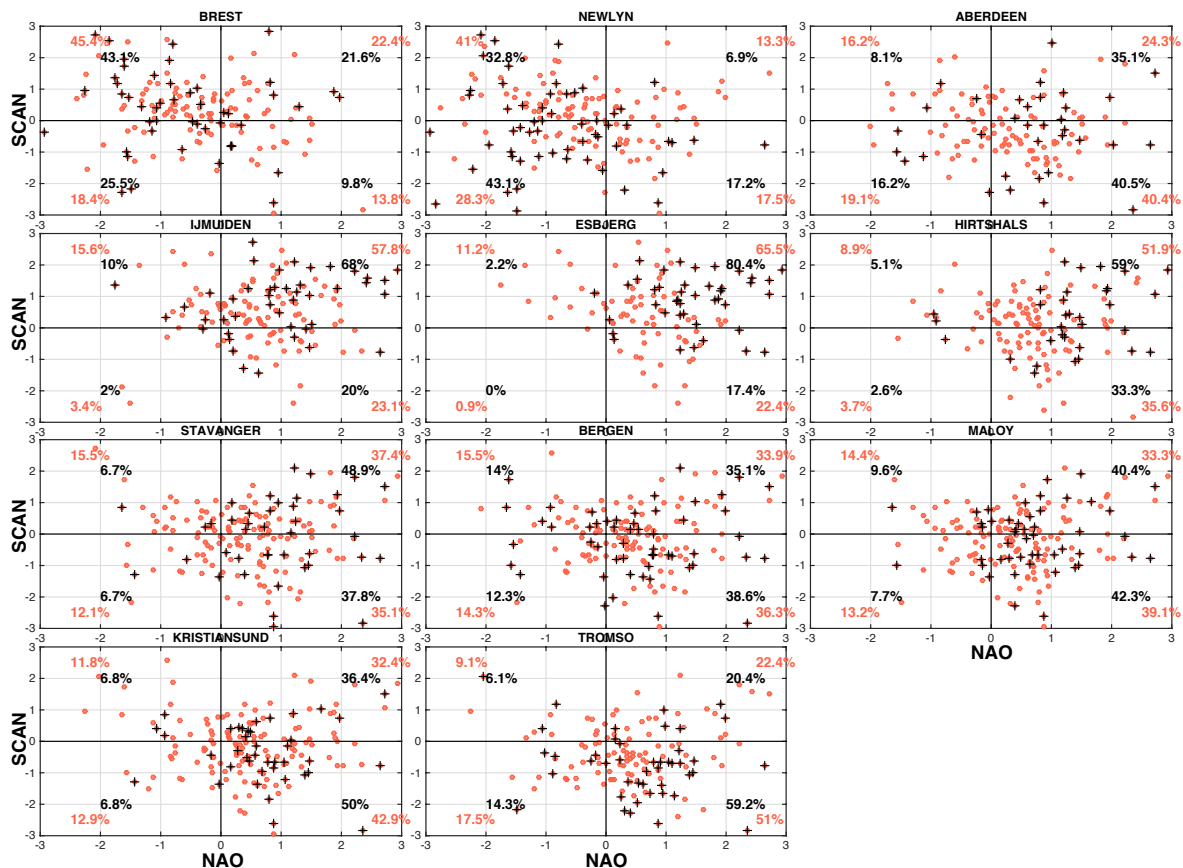


**Figure 10.** Anomalously/extremely high (red circles/black crosses) monthly sea levels recorded at the different TGs along the European coasts projected onto the NAO-SCAN teleconnection space. The threshold value for the anomalous/extreme monthly sea levels is 0.75/1.5 std. The percentages represent the number of anomalously/extremely high (in red/black) months in every quadrant divided by the total number of anomalously high/extreme months in all quadrants.

It is evident that anomalous sea-level variations at every TG is associated with a unique atmospheric state and pattern combination. We have, however, in Figure 11 identified three TG regions with common large-scale circulation patterns. At the Norwegian tide gauges, the anomalous monthly sea levels are dominated by an MSLP gradient between the Irminger Sea and central Europe. The North Sea tide gauges, apart from Aberdeen, project onto a north-south pressure gradient with nodes over northern Scandinavia and in the vicinity of the Bay of Biscay. Newlyn and Brest are associated with markedly poleward shifted centers of action, but are clearly dominated by the low-pressure (southern center of action) encompassing the subpolar North Atlantic. It is, however, important to keep in mind that at this stage the inverted barometric effect has been removed, so that this solely represents wind forcing. A key point to conclude with from this analysis is that the patterns driving the anomalous sea

level variability at each tide gauge are different from the NAO dipole, and can only be understood in terms of the combinations with the other two teleconnection patterns, EAP and SCAN.

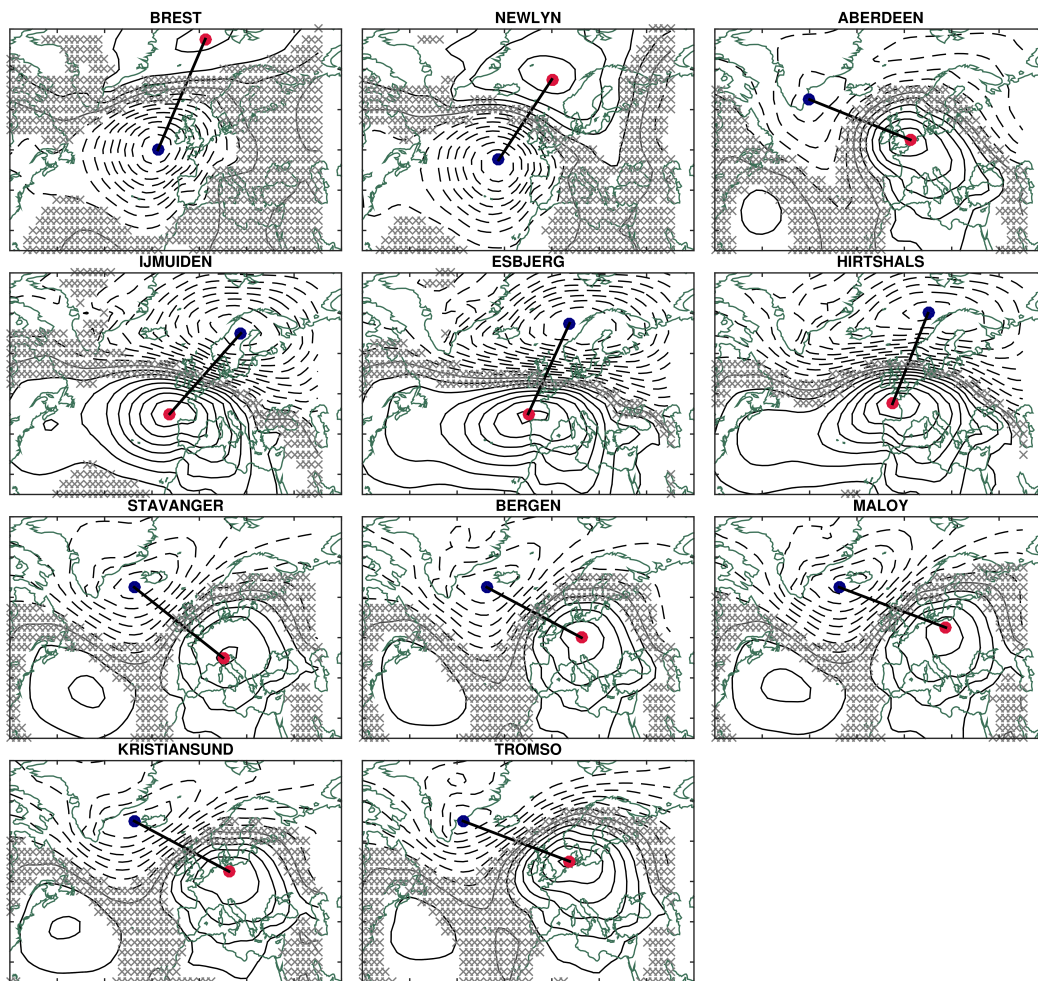


**Figure 11.** Composite difference of MSLP based on anomalous monthly sea levels from different TGs along the European coasts. The threshold value for the anomalous monthly TG sea levels is 0.75 std. Anomalously positive and negative MSLP is indicated by solid and dashed contours with a spacing of 1 hPa. The red and blue dots are assigned to the lowest and highest MSLP anomaly, respectively. The non-significant regions below the 99% confidence level are indicated by gray crosses calculated using a two-sided *t* test.

### 3.5. Coherent European Sea Level Variability

We have so far dealt with understanding anomalous monthly sea levels on a regional and local scale, however, in this section we make an attempt to represent the European shelves/coasts using a single index. Figure 12a shows the first leading EOF of monthly sea level variability on the European shelf only using altimetry. The spatial pattern of the leading EOF is notably a monopole with a node over the North Sea and explains about 51% of the variance. The associated first Principal Component (PC1) is shown in Figure 12b, where the anomalous months (using threshold value of 0.75 std) are highlighted. Figure 12c shows the PC1 based on the 11 European TGs displayed in Figure 1. The comparison between PC1 based on TGs and that from altimetry is good with a correlation of 0.71. This result suggests that the on-shelf PC1 is a good proxy that captures the sea-level variations along the European coast from TGs.

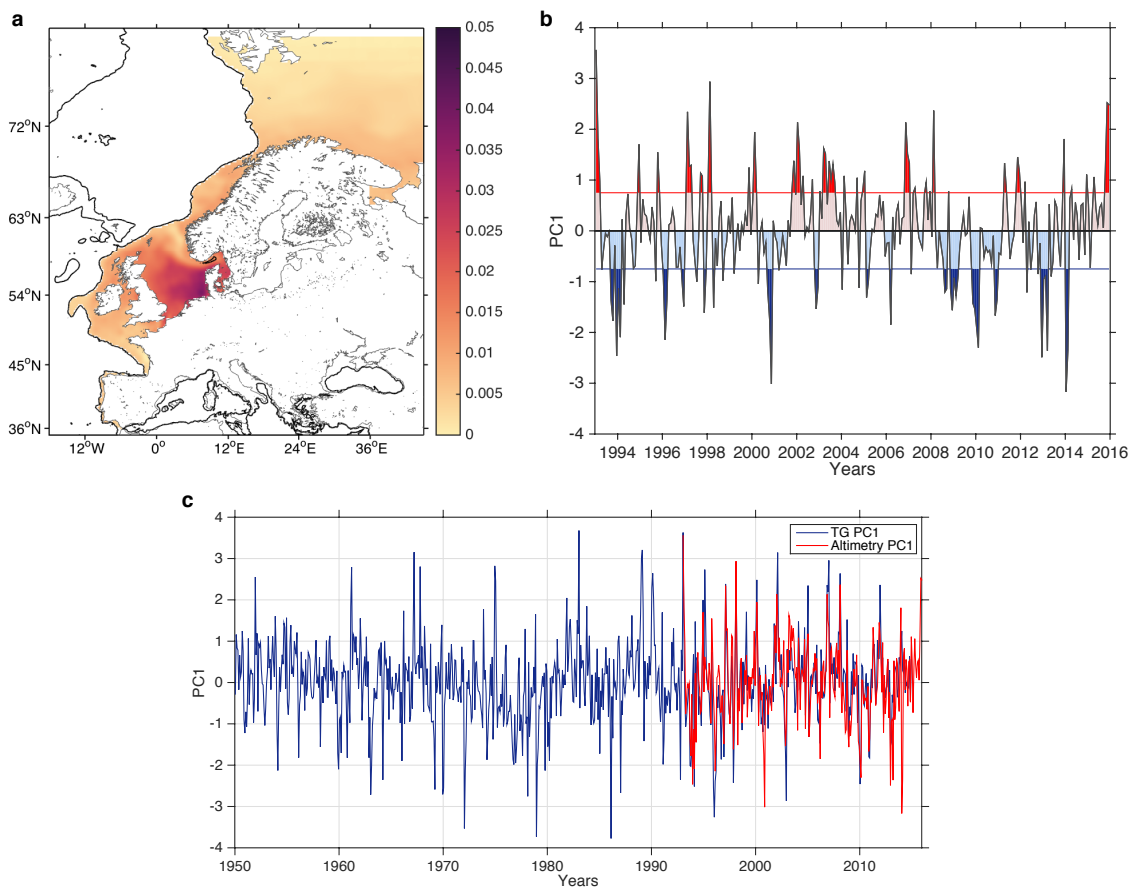


**Figure 12.** (a) First EOF of the monthly on-shelf sea level from altimetry (1993–2015). (b) The PC1 associated with the first EOF of the on-shelf sea level. (c) PC1 (blue) derived based on the 11 tide gauges (1950–2014) displayed in Figure 1 and overlaid by the on-shelf PC1 (red). The on-shelf and TG PC1 explains 51% and 61% of the variance, respectively. The correlation between the on-shelf and TG PCs is 0.71.

We will now explore the sea level and the atmospheric circulation patterns associated with anomalous monthly sea levels based on the on-shelf and TG PC1s. Figure 13a shows a composite difference between anomalously high and low on-shelf sea level. The highest amplitudes are found in the Barents, Norwegian shelf and North Sea and by the British Isles, and comparatively smaller amplitudes in the Bay of Biscay. Figure 13a further shows that the atmospheric centers of action are centered over Brest and the Barents Sea, respectively. The sea level and atmospheric circulation patterns projecting on the TG PC1 (Figure 13b) show similar features and are hence consistent with those based on the on-shelf PC1 (not surprising considering the strong correlation between these PC1s). These results suggest that due to this poleward and eastward reorganization (relative to the climatological NAO position) of the atmospheric circulation, the winds are nearly parallel to the continental slope all the way from the Bay of Biscay to northern Norway (longshore winds), which through Ekman transport and convergence towards the coast increases the sea level coherently along the European coast, as portrayed in Figure 13c. Coherent coastal sea level variability is thus dependent on the strength and direction of the winds controlled by migrations of the North Atlantic meridional pressure dipole.

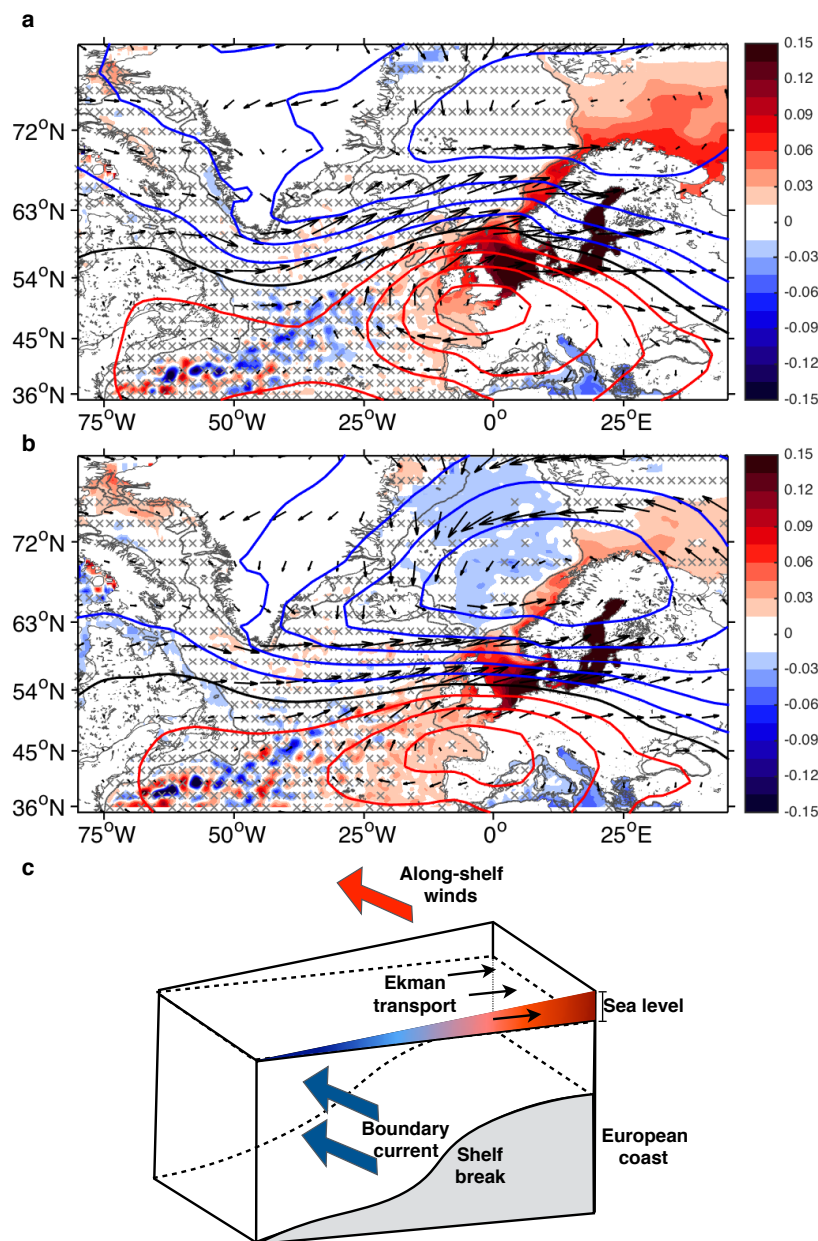


**Figure 13.** Composite difference of sea level from altimetry (m, shading), MSLP (hPa, contours) and 10 m winds (arrows) based on (a) the on-shelf and (b) the TG PC1s. The sea level, MSLP and winds have deseasoned and detrended before the composite analysis, which is based on the difference between anomalously high ( $>0.75$  std) and low ( $<-0.75$  std) periods in the PC1s. The black contour denotes the zero MSLP anomaly, while the blue/red contours denote negative/positive MSLP anomaly with a spacing of 2 hPa. (c) Schematic diagram including the main dynamical processes involved on monthly timescales. This case reflects southerly along-shelf/shore winds that through Ekman transports increase the coastal sea level. The non-significant regions below the 95% confidence level are indicated by gray crosses calculated using a two-sided  $t$  test.

The overall pattern driving the sea level variability at the European coasts is reminiscent of that associated with NAO+/SCAN+ (Figure 4b). We project, as above, these anomalous months onto the space spanned by the NAO and SCAN indices to investigate their distribution, cf. Figure 14. The main conclusion is that the anomalously high monthly sea levels of the on-shelf and TG PC1 are predominantly governed by NAO+/SCAN+ pattern, more than the NAO interplay with the

EAP (about ~9% difference between NAO+/EAP– and NAO+/EAP+ for both the anomalously and extremely high monthly sea levels, not shown).

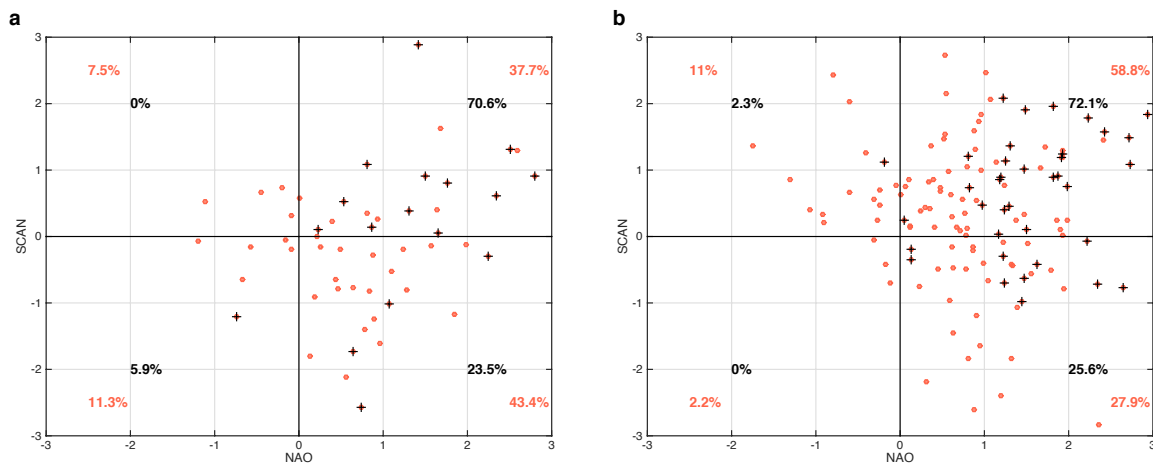


**Figure 14.** Anomalously/extremely high (red circles/black crosses) monthly sea levels based on (a) the on-shelf first Principal Component (PC1) constructed from altimetry, and (b) TG PC1, projected onto the NAO-SCAN teleconnection space. The percentages represent the number of anomalously/extremely (>0.75/1.5 std) high (in red/black) months in every quadrant divided by the total number of anomalously high/extreme months in all quadrants.

#### 4. Summarizing Discussion and Outlook

Atmospheric forcing has long been recognized as the dominant forcing factor of sea level variability over the Northern European Shelf. The physical connection between atmospheric forcing and sea level expresses itself through a strong, but non-stationary link to the NAO. The location of the centers of action associated with the North Atlantic meridional pressure dipole, however, can be affected through the interplay with the EAP and SCAN teleconnections, potentially explaining the temporally-varying relationship between sea level variability and the NAO. Our results indicate that it is indeed important to account for the binary interaction of the NAO with EAP/SCAN to better understand the drivers inducing anomalous sea level periods along the European coast.

Our analysis was divided into three main parts. First, we demonstrated that the spatial movements of the centers of action can be captured through the combination of the NAO with the second or third leading EOF of atmospheric variability in the North Atlantic/European sector [14,28]. Apart from explaining the spatial migrations of the North Atlantic meridional pressure dipole, the binary patterns are able to modulate the strength of the MSLP at the centers of action and hence the wind speeds, which, in turn, further influences the sea level. Second, we showed that these combinations can explain the regional sea level differences along the European shelves and coasts, with consistent results from altimetry and tide gauges. It should, however, be mentioned that these regional differences are likely first induced by the NAO, but they are greatly enhanced under the influence of the other two teleconnection patterns. Tsimplis and Shaw [37] note, for example, that if the effect of the NAO and hence westerly winds are removed (regressed out) from the mean sea level at tide gauges around Europe, a weakened relationship between the regions is found. Third, we constructed an index that represent the entire European shelves/coasts, which is found to project on an MSLP dipole pattern with nodes over northwestern Scandinavia and the Bay of Biscay. This modified dipole pattern organizes the winds such that they trace the continental shelf break from the Bay of Biscay all the way to northern Norway. The teleconnection space revealed that the majority of anomalously high sea levels in the tide gauge based index (TG PC1) corresponded to positive phases of both the NAO and the SCAN and the

combination of these teleconnections can thus be concluded to be the atmospheric pattern that most strongly induces coherent sea level variability along the European shelves and coasts (Figure 13).

The relationship between the NAO and sea level from tide gauges in the North Sea has been suggested by several studies to be highly variable with time, which is presumed to be due to the movements of the centers of action dominating different periods [12,31,33,34]. As shown by Hilmer and Jung [40], the centers of action was shifted eastwards during the 1978–1997 period as compared to the 1958–1977 period. Although not mentioned by these investigators, a close inspection of their results suggests that the mean 1978–1997 atmospheric state mirrors the NAO+/SCAN+ combination. This is corroborated by Moore et al. [14], where both the NAO and SCAN indices are shown to have been on the positive side over low-frequency timescales (cf. their Figure 8). An NAO+/SCAN+ situation leads to a clockwise shift of the centers of action with the low-pressure node being located slightly west of Norway, which strongly resembles the mean 1978–1997 atmospheric state shown by Hilmer and Jung [40] (see also Comas-Bru and McDermott [23] and Kolker and Hameed [42]). With respect to our results, we note that the majority of the anomalously high monthly sea levels at the North Sea TGs are induced by the NAO+/SCAN+ type of pattern (Figure 10), which may further suggest that the persistency of a same sign NAO-SCAN pattern is likely to reinforce this time-varying relationship between the atmospheric circulation and sea level. We conclude that the NAO+/SCAN+ combination may have induced this multidecadal shift in the location of the centers of action and as a result the correlation with the sea level in the North Sea and Baltic Seas was diagnosed to be higher. Therefore, our results could potentially be valuable if applied to sea level variations on longer timescales.

We note that the atmospheric circulations patterns inducing anomalous or extreme monthly sea levels along the European coast (when represented by a single index) based on both altimetry and TGs were similar (Figures 12 and 13). However, a close inspection of these patterns reveals some differences, although as shown in Figures 13 and 14, both the on-shelf and TG PCs are primarily associated with NAO+/SCAN+ type of pattern (Figure 4). The major difference is that the altimetric on-shelf PC1 projects onto an MSLP dipole pattern that is more shifted polewards (as compared to the pattern based on the TG PC1) with a low-pressure node close to the Barents Sea opening and a high-pressure node more-or-less close to Brest. This overall shift polewards can be seen to drive alongshelf/shore winds following the 500 m isobath from the Bay of Biscay all the way the Barents Sea opening. The TG PC1, however, projects onto an MSLP pattern that organizes the isobars in a zonal manner across the North Sea. One reason causing this pattern difference may in fact lie in our altimetric EOF analysis which, unlike the TG EOF analysis (note that northernmost station is Tromsø), accounts for the Barents Sea region. Furthermore, the atmospheric pattern based on TGs bears a strong resemblance to that reported to correlate well with the monthly mean sea level variability from 13 TGs in the German Bight region [13]. Dangendorf et al. [13] constructed a proxy based on MSLP over Scandinavia and the Iberian Peninsula, and found that it explained about 80% (as compared to the 30–35% explained by the NAO) of the variability and concluded, in addition, that this proxy is capable of reproducing the decadal mean sea-level fluctuations in the German Bight. The present study thus provides a better understanding of the pattern in Dangendorf et al. [13] by revealing that it emerges as a result of the interplay between the NAO and the SCAN (Figure 14b).

Anomalous and extreme monthly sea levels along the Norwegian coast evidently respond to the EAP, but there are some differences within this coastal zone. This applies, in particular, to the northernmost TGs, which are found to be more sensitive to the SCAN than to the EAP (cf. Figures 9 and 10). In contrast, for the North Sea, although dominated by the SCAN, we note that a non-negligible portion of anomalous and extreme monthly sea levels responds to the negative phase of the EAP as well. Due to the clockwise displacement and poleward shift of the North Atlantic meridional pressure dipole, the pattern associated with NAO+/EAP– has its zero-line crossing the North Sea, resulting in a situation that enhances the westerly winds and thereby induces anomalously high/extreme sea levels there. Thus, the North Sea TGs analyzed here are sensitive to both the phase

of the SCAN and the EAP. Based on this conclusion, we asked ourselves whether it would not have been feasible to combine all three EOFs. That we did not conduct this type of analysis is, however, not a limitation since we found that the mobility of the North Atlantic meridional pressure dipole due to either the EAP or SCAN separately provides a dynamically clearer picture regarding their impact on sea level, which further acts a simple guideline of what to expect when two EOFs are combined (Figures 3, 4 and 8).

The schematics in Figure 13c depicts that the eastern boundary current locked to the continental slope is further enhanced by the same atmospheric circulation that induce anomalously high sea levels along the European shelves and coasts through geostrophic dynamics. Richter et al. [49] modelled the boundary current at one location (Svinøy) using the across-slope sea level gradient from tide gauges between the Norwegian west coast and the Faroe Islands and found a good correlation of 0.6. We think that the altimetric on-shelf or TG PC1 may be useful to reconstruct the variability of this boundary current, and that these binary combinations may further elucidate the drivers, which have solely been investigated in terms of the NAO (see, e.g., Skagseth et al. [50], Sandø et al. [51], Chafik et al. [52]). Furthermore, the European shelves respond on decadal timescales to open-ocean steric height variations [11,53], which may impact the across-slope sea level gradient and hence regulate the strength of the boundary current. Thus, the on-shelf or TG PC1 may further be useful to better understand the low-frequency variability of the nearly-barotropic shelf-edge current that carries Atlantic water to the Arctic, especially in the Nordic Seas region.

Our objective has been to understand the impact of North Atlantic teleconnections on northern European sea levels with less focus on the forcing mechanisms of these teleconnections, and the reader is referred to, e.g., Cassou et al. [48] for details (see also [54–58]). But, to shed some light on this issue, we apply a similar composite analysis as in Figure 13 on additional key variables and show the hemispheric-scale linkages (Figure 15). The main picture that emerges is that anomalously high northern European monthly sea levels (Figure 15a) coincide with a tripolar pattern of sea surface temperature (SST) anomalies extending across the North Atlantic and a warm SST anomaly in the central tropical Pacific (Figure 15b). These pronounced SST anomalies vary simultaneously with the upper-troposphere geopotential height anomalies (Figure 15c). A recent study by Schemm et al. [57] demonstrates that warm SST anomalies over these two key regions, i.e., central tropical Pacific and Gulf Stream, promote a more northeastward North Atlantic storm track (as anticipated during anomalous NAO+/SCAN+ periods, cf. Figure 13). In particular, they report that synchronously with central (eastern) Pacific El Niño winters, the cyclogenesis location over the Gulf Stream region is located north of its climatological position, which, in turn, steers the storm tracks into a northeastward (zonal) path across the Atlantic. In fact, they calculate that ~20–25% (2–3%) of the cyclones that originate from the Gulf Stream traverse the northern Nordic Seas region during active central (eastern) Pacific El Niño winters. Furthermore, the warm SST anomaly that normally accompanies a northward shift of the Gulf Stream current system has recently been suggested to be a key factor for triggering the SCAN teleconnection pattern through enhanced transient eddy vorticity flux [58]. Taken together, these results suggest that the North Atlantic tripolar SST pattern and its associated Rossby wave train (Figure 15b) emanating from the Gulf Stream region and connecting the western North Atlantic with the European sector is a potential source, likely also in combination with central Pacific El Niños, for triggering the teleconnection pattern driving anomalous monthly European sea levels. More research along these lines is thus warranted to better understand the global-scale drivers of European sea level change.

In a warming climate, the position of the centers of action associated with the North Atlantic meridional pressure dipole are projected to shift slightly northeastward and amplify by the end of the twenty-first century [59]. Such a change would dynamically push the European mean sea level to a higher state as well as increase the extreme monthly sea levels as this northeastward shift is reported to be associated with deeper cyclones under increasing anthropogenic climate change conditions (see, e.g., Pinto et al. [60], Feser et al. [61]). Therefore, even a future small shift in the position of

the North Atlantic meridional pressure dipole may lead to large effects on European sea levels and hence enhanced flood risk, further underlining that a correct representation of these atmospheric teleconnections in climate models is a prerequisite for projecting sea level change, in particular, on the regional scale. Not least since the variability caused by the interaction of the teleconnection patterns demonstrated herein are on the order of magnitude as the centennial global mean sea level change [1]. Furthermore, on a national level these combinations may act as a guideline of which atmospheric patterns and concomitant teleconnection states are important. As we have demonstrated in the present study, it may not be sufficient to only predict the NAO (see, e.g., Scaife et al. [55]). Seasonal forecasts of the EAP and SCAN, which have been suggested to be linked to tropical Pacific and North Atlantic sea surface temperature variability [62,63], would be valuable to the European coastal communities.

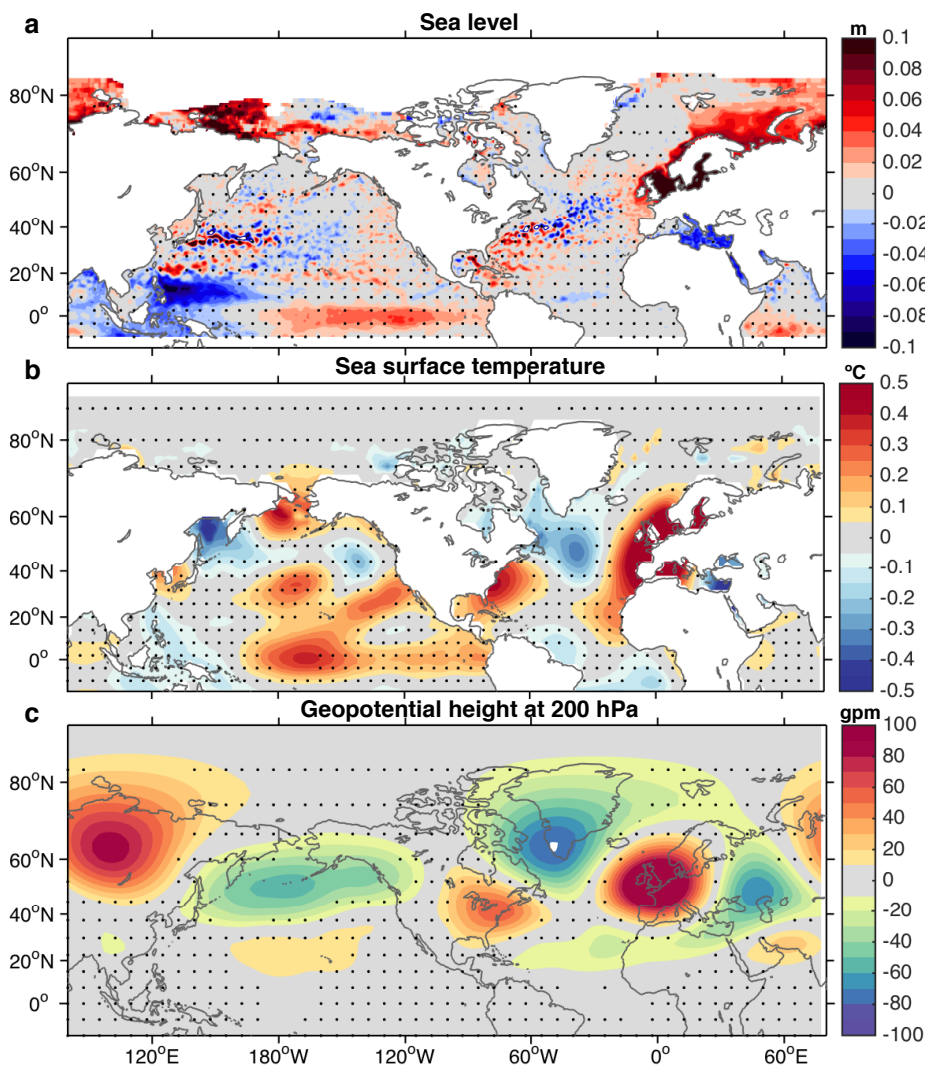


**Figure 15.** Composite difference of (a) sea level (m), (b) sea surface temperature (SST) (°C) and (c) non-zonal geopotential height (at 200 hPa) anomalies (gpm) based on the difference between anomalously high (>0.75 std) and low (<-0.75 std) periods of the on-shelf PC1 (1993–2015). The SST data is based on the extended reconstructed sea surface temperature version 4 (ERSSTv4) [64]. The geopotential height is from the NCEP/NCAR reanalysis [46]. The data have been deseasoned and detrended before the analysis. The stipplings indicate non-significant regions below the 95% confidence level using a two-sided *t* test.

**Acknowledgments:** This work was funded by the Centre for Climate Dynamics at the Bjerknes Centre, through the project iNCREASE. S.D. would like to thank the University of Siegen. The altimeter products were produced by Ssalto/Duacs and distributed by Aviso, with support from Cnes (<http://www.aviso.altimetry.fr/duacs/>). We thank PSMSL for the tide gauge data. We would like to thank three anonymous reviewers for valuable comments that improved the paper.

**Author Contributions:** L.C., J.E.O.N. and S.D. conceived and designed the analysis; L.C. conducted the analysis and wrote the paper; all authors contributed to the writing of the paper.

**Conflicts of Interest:** The authors declare no conflict of interest.

## Abbreviations

The following abbreviations are used in this manuscript:

|           |   |
|-----------|---|
| NAO       | North Atlantic Oscillation  |
| EAP       | East Atlantic Pattern   |
| SCAN      | Scandinavian Pattern  |
| DUACS     | Data Unification and Altimeter Combination System                                     |
| DT2014    | Delayed Time 2014   |
| MDT       | Mean Dynamic Topography   |
| CNES/CLS  | Centre national d'études spatiales/Collecte Localisation Satellites                   |
| NCEP/NCAR | National Center for Environmental Prediction/National Center for Atmospheric Research |
| EOF       | Empirical Orthogonal Functions  |
| PC1       | First Principal Component   |
| TG        | Tide Gauges   |
| PSMSL     | Permanent Service for Mean Sea Level  |
| SST       | Sea Surface Temperature   |
| ERSSTv4   | Extended Reconstructed Sea Surface Temperature version 4                              |

## References

- Dangendorf, S.; Marcos, M.; Wöppelmann, G.; Conrad, C.P.; Frederikse, T.; Riva, R. Reassessment of 20th century global mean sea level rise. *Proc. Natl. Acad. Sci. USA* **2017**, *114*, doi:10.1073/pnas.1616007114.
- Cazenave, A.; Dieng, H.B.; Meyssignac, B.; Von Schuckmann, K.; Decharme, B.; Berthier, E. The rate of sea-level rise. *Nat. Clim. Chang.* **2014**, *4*, 358–361.
- Bindoff, N.L.; Willebrand, J.; Artale, V.; Cazenave, A.; Gregory, J.M.; Gulev, S.; Hanawa, K.; Le Quéré, C.; Levitus, S.; Nojiri, Y.; et al. Observations: Oceanic Climate Change and Sea Level. In *Climate Change 2007: The Physical Science Basis*; Cambridge University Press: Cambridge, UK; New York, NY, USA, 2007.
- Church, J.A.; Clark, P.U.; Cazenave, A.; Gregory, J.M.; Jevrejeva, S.; Levermann, A.; Merrifield, M.A.; Milne, G.A.; Nerem, R.S.; Nunn, P.D.; et al. Sea-level rise by 2100. *Science* **2013**, *342*, 1445.
- Nicholls, R.J.; Cazenave, A. Sea-level rise and its impact on coastal zones. *Science* **2010**, *328*, 1517–1520.
- Kopp, R.E.; Horton, R.M.; Little, C.M.; Mitrovica, J.X.; Oppenheimer, M.; Rasmussen, D.; Strauss, B.H.; Tebaldi, C. Probabilistic 21st and 22nd century sea-level projections at a global network of tide-gauge sites. *Earth's Future* **2014**, *2*, 383–406.
- Carson, M.; Köhl, A.; Stammer, D.; Slangen, A.; Katsman, C.; Van de Wal, R.; Church, J.; White, N. Coastal sea level changes, observed and projected during the 20th and 21st century. *Clim. Chang.* **2016**, *134*, 269–281.
- Slangen, A.; Adloff, F.; Jevrejeva, S.; Leclercq, P.; Marzeion, B.; Wada, Y.; Winkelmann, R. A review of recent updates of sea-level projections at global and regional scales. *Surv. Geophys.* **2016**, *38*, 385–406.
- Sturges, W.; Douglas, B.C. Wind effects on estimates of sea level rise. *J. Geophys. Res. Oceans* **2011**, *116*, doi:10.1029/2010JC006492.
- Calafat, F.; Chambers, D.; Tsimplis, M. Mechanisms of decadal sea level variability in the eastern North Atlantic and the Mediterranean Sea. *J. Geophys. Res. Oceans* **2012**, *117*, doi:10.1029/2012JC008285.
- Dangendorf, S.; Calafat, F.M.; Arns, A.; Wahl, T.; Haigh, I.D.; Jensen, J. Mean sea level variability in the North Sea: Processes and implications. *J. Geophys. Res. Oceans* **2014**, *119*, doi:10.1002/2014JC009901.
- Wakelin, S.; Woodworth, P.; Flather, R.; Williams, J. Sea-level dependence on the NAO over the NW European Continental Shelf. *Geophys. Res. Lett.* **2003**, *30*, doi:10.1029/2003GL017041.

13. Dangendorf, S.; Wahl, T.; Nilson, E.; Klein, B.; Jensen, J. A new atmospheric proxy for sea level variability in the southeastern North Sea: Observations and future ensemble projections. *Clim. Dyn.* **2014**, *43*, 447–467.
14. Moore, G.W.K.; Renfrew, I.A.; Pickart, R.S. Multidecadal Mobility of the North Atlantic Oscillation. *J. Clim.* **2012**, *26*, 2453–2466.
15. Hurrell, J.W. Decadal Trends in the North Atlantic Oscillation: Regional Temperatures and Precipitation. *Science* **1995**, *269*, 676–679.
16. Stephenson, D.B.; Pavan, V.; Bojariu, R. Is the North Atlantic Oscillation a random walk? *Int. J. Clim.* **2000**, *20*, 1–18.
17. Nilsen, J.; Gao, Y.; Drange, H.; Furevik, T.; Bentsen, M. Simulated North Atlantic-Nordic Seas water mass exchanges in an isopycnic coordinate OGCM. *Geophys. Res. Lett.* **2003**, *30*, doi:10.1029/2002GL016597.
18. Furevik, T.; Nilsen, J.E.Ø. Large-Scale Atmospheric Circulation Variability and its Impacts on the Nordic Seas Ocean Climate—A Review. In *The Nordic Seas: An Integrated Perspective*; American Geophysical Union: Washington, DC, USA, 2005; pp. 105–136.
19. Moore, G.; Pickart, R.; Renfrew, I. Complexities in the climate of the subpolar North Atlantic: A case study from the winter of 2007. *Q. J. R. Meteorol. Soc.* **2011**, *137*, 757–767.
20. Castelle, B.; Dodet, G.; Masselink, G.; Scott, T. A new climate index controlling winter wave activity along the Atlantic coast of Europe: The West Europe Pressure Anomaly. *Geophys. Res. Lett.* **2017**, *44*, 1384–1392.
21. Fereday, D.; Knight, J.; Scaife, A.; Folland, C.; Philipp, A. Cluster analysis of North Atlantic–European circulation types and links with tropical Pacific sea surface temperatures. *J. Clim.* **2008**, *21*, 3687–3703.
22. Moore, G.W.K.; Renfrew, I.A. Cold European winters: Interplay between the NAO and the East Atlantic mode. *Atmos. Sci. Lett.* **2012**, *13*, 1–8.
23. Comas-Bru, L.; McDermott, F. Impacts of the EA and SCA patterns on the European twentieth century NAO–winter climate relationship. *Q. J. R. Meteorol. Soc.* **2013**, *140*, 354–363.
24. Bastos, A.; Janssens, I.; Gouveia, C.; Trigo, R.; Ciais, P.; Chevallier, F.; Peñuelas, J.; Rödenbeck, C.; Piao, S.; Friedlingstein, P.; et al. European land CO<sub>2</sub> sink influenced by NAO and East-Atlantic Pattern coupling. *Nat. Commun.* **2016**, *7*, 10315.
25. Wallace, J.M.; Gutzler, D.S. Teleconnections in the Geopotential Height Field during the Northern Hemisphere Winter. *Mon. Weather Rev.* **1981**, *109*, 784–812.
26. Barnston, A.G.; Livezey, R.E. Classification, Seasonality and Persistence of Low-Frequency Atmospheric Circulation Patterns. *Mon. Weather Rev.* **1987**, *115*, 1083–1126.
27. Bueh, C.; Nakamura, H. Scandinavian pattern and its climatic impact. *Q. J. R. Meteorol. Soc.* **2007**, *133*, 2117–2131.
28. Franzke, C.; Feldstein, S.B. The continuum and dynamics of Northern Hemisphere teleconnection patterns. *J. Atmos. Sci.* **2005**, *62*, 3250–3267.
29. Rossby, C.G. Relation between variations in the intensity of the zonal circulation of the atmosphere and the displacements of the semi-permanent centers of action. *J. Mar. Res.* **1939**, *2*, 38–55.
30. Woollings, T.; Hannachi, A.; Hoskins, B. Variability of the North Atlantic eddy-driven jet stream. *Q. J. R. Meteorol. Soc.* **2010**, *136*, 856–868.
31. Andersson, H.C. Influence of long-term regional and large-scale atmospheric circulation on the Baltic sea level. *Tellus A* **2002**, *54*, 76–88.
32. Woolf, D.K.; Shaw, A.G.; Tsimplis, M.N. The influence of the North Atlantic Oscillation on sea-level variability in the North Atlantic region. *Glob. Atmos. Ocean Syst.* **2003**, *9*, 145–167.
33. Yan, Z.; Tsimplis, M.N.; Woolf, D. Analysis of the relationship between the North Atlantic oscillation and sea-level changes in northwest Europe. *Int. J. Clim.* **2004**, *24*, 743–758.
34. Jevrejeva, S.; Moore, J.; Woodworth, P.; Grinsted, A. Influence of large-scale atmospheric circulation on European sea level: Results based on the wavelet transform method. *Tellus A* **2005**, *57*, 183–193.
35. Papadopoulos, A.; Tsimplis, M. Coherent coastal sea-level variability at interdecadal and interannual scales from tide gauges. *J. Coast. Res.* **2006**, *22*, 625–639.
36. Woodworth, P.; Flather, R.; Williams, J.; Wakelin, S.; Jevrejeva, S. The dependence of UK extreme sea levels and storm surges on the North Atlantic Oscillation. *Cont. Shelf Res.* **2007**, *27*, 935–946.
37. Tsimplis, M.N.; Shaw, A.G. The forcing of mean sea level variability around Europe. *Glob. Planet. Chang.* **2008**, *63*, 196–202.

38. Dangendorf, S.; Wahl, T.; Hein, H.; Jensen, J.; Mai, S.; Mudersbach, C. Mean sea level variability and influence of the North Atlantic Oscillation on long-term trends in the German Bight. *Water* **2012**, *4*, 170–195.
39. Chen, X.; Dangendorf, S.; Narayan, N.; O'Driscoll, K.; Tsimplis, M.N.; Su, J.; Mayer, B.; Pohlmann, T. On sea level change in the North Sea influenced by the North Atlantic Oscillation: Local and remote steric effects. *Estuar. Coast. Shelf Sci.* **2014**, *151*, 186–195.
40. Hilmer, M.; Jung, T. Evidence for a recent change in the link between the North Atlantic Oscillation and Arctic sea ice export. *Geophys. Res. Lett.* **2000**, *27*, 989–992.
41. Jung, T.; Hilmer, M.; Ruprecht, E.; Kleppek, S.; Gulev, S.K.; Zolina, O. Characteristics of the recent eastward shift of interannual NAO variability. *J. Clim.* **2003**, *16*, 3371–3382.
42. Kolker, A.S.; Hameed, S. Meteorologically driven trends in sea level rise. *Geophys. Res. Lett.* **2007**, *34*, doi:10.1029/2007GL031814.
43. Ullmann, A.; Monbaliu, J. Changes in atmospheric circulation over the North Atlantic and sea-surge variations along the Belgian coast during the twentieth century. *Int. J. Clim.* **2010**, *30*, 558–568.
44. Pujol, M.I.; Faugère, Y.; Taburet, G.; Dupuy, S.; Pelloquin, C.; Ablain, M.; Picot, N. DUACS DT2014: The new multi-mission altimeter data set reprocessed over 20 years. *Ocean Sci.* **2016**, *12*, 1067–1090.
45. Holgate, S.J.; Matthews, A.; Woodworth, P.L.; Rickards, L.J.; Tamisiea, M.E.; Bradshaw, E.; Foden, P.R.; Gordon, K.M.; Jevrejeva, S.; Pugh, J. New data systems and products at the permanent service for mean sea level. *J. Coast. Res.* **2013**, *29*, 493–504.
46. Kalnay, E.; Kanamitsu, M.; Kistler, R.; Collins, W.; Deaven, D.; Gandin, L.; Iredell, M.; Saha, S.; White, G.; Woollen, J.; et al. The NCEP/NCAR 40-Year Reanalysis Project. *Bull. Am. Meteorol. Soc.* **1996**, *77*, 437–471.
47. Hannachi, A.; Jolliffe, I.T.; Stephenson, D.B. Empirical orthogonal functions and related techniques in atmospheric science: A review. *Int. J. Clim.* **2007**, *27*, 1119–1152.
48. Cassou, C.; Terray, L.; Hurrell, J.W.; Deser, C. North Atlantic winter climate regimes: Spatial asymmetry, stationarity with time, and oceanic forcing. *J. Clim.* **2004**, *17*, 1055–1068.
49. Richter, K.; Segtnan, O.H.; Furevik, T. Variability of the Atlantic inflow to the Nordic Seas and its causes inferred from observations of sea surface height. *J. Geophys. Res. Oceans* **2012**, *117*, C04004.
50. Skagseth, Ø.; Orvik, K.A.; Furevik, T. Coherent variability of the Norwegian Atlantic Slope Current derived from TOPEX/ERS altimeter data. *Geophys. Res. Lett.* **2004**, *31*, L14304.
51. Sandø, A.; Nilsen, J.; Eldevik, T.; Bentsen, M. Mechanisms for variable North Atlantic–Nordic seas exchanges. *J. Geophys. Res. Oceans* **2012**, *117*, doi:10.1029/2012JC008177.
52. Chafik, L.; Nilsson, J.; Skagseth, Ø.; Lundberg, P. On the flow of Atlantic water and temperature anomalies in the Nordic Seas toward the Arctic Ocean. *J. Geophys. Res. Oceans* **2015**, *120*, 7897–7918.
53. Frederikse, T.; Riva, R.; Slobbe, C.; Broerse, T.; Verlaan, M. Estimating decadal variability in sea level from tide gauge records: An application to the North Sea. *J. Geophys. Res. Oceans* **2016**, *121*, 1529–1545.
54. Li, Y.; Lau, N.C. Impact of ENSO on the atmospheric variability over the North Atlantic in late winter—Role of transient eddies. *J. Clim.* **2012**, *25*, 320–342.
55. Scaife, A.; Arribas, A.; Blockley, E.; Brookshaw, A.; Clark, R.; Dunstone, N.; Eade, R.; Fereday, D.; Folland, C.; Gordon, M.; et al. Skillful long-range prediction of European and North American winters. *Geophys. Res. Lett.* **2014**, *41*, 2514–2519.
56. Drouard, M.; Rivière, G.; Arbogast, P. The link between the North Pacific climate variability and the North Atlantic Oscillation via downstream propagation of synoptic waves. *J. Clim.* **2015**, *28*, 3957–3976.
57. Schemm, S.; Ciasto, L.M.; Li, C.; Kvamstø, N.G. Influence of tropical Pacific sea surface temperature on the genesis of Gulf Stream cyclones. *J. Atmos. Sci.* **2016**, *73*, 4203–4214.
58. Jung, O.; Sung, M.K.; Sato, K.; Lim, Y.K.; Kim, S.J.; Baek, E.H.; Jeong, J.H.; Kim, B.M. How does the SST variability over the western North Atlantic Ocean control Arctic warming over the Barents–Kara Seas? *Environ. Res. Lett.* **2017**, *12*, 034021.
59. Ulbrich, U.; Christoph, M. A shift of the NAO and increasing storm track activity over Europe due to anthropogenic greenhouse gas forcing. *Clim. Dyn.* **1999**, *15*, 551–559.
60. Pinto, J.G.; Zacharias, S.; Fink, A.H.; Leckebusch, G.C.; Ulbrich, U. Factors contributing to the development of extreme North Atlantic cyclones and their relationship with the NAO. *Clim. Dyn.* **2009**, *32*, 711–737.
61. Feser, F.; Barcikowska, M.; Krueger, O.; Schenk, F.; Weisse, R.; Xia, L. Storminess over the North Atlantic and northwestern Europe—A review. *Q. J. R. Meteorol. Soc.* **2015**, *141*, 350–382.

62. Iglesias, I.; Lorenzo, M.N.; Taboada, J.J. Seasonal predictability of the East atlantic pattern from sea surface temperatures. *PLoS ONE* **2014**, *9*, e86439.
63. King, M.P.; Herceg-Bulić, I.; Kucharski, F.; Keenlyside, N. Interannual tropical Pacific sea surface temperature anomalies teleconnection to Northern Hemisphere atmosphere in November. *Clim. Dyn.* **2017**, 1–19, doi:10.1007/s00382-017-3727-5.
64. Huang, B.; Thorne, P.W.; Smith, T.M.; Liu, W.; Lawrimore, J.; Banzon, V.F.; Zhang, H.M.; Peterson, T.C.; Menne, M. Further exploring and quantifying uncertainties for extended reconstructed sea surface temperature (ERSST) version 4 (v4). *J. Clim.* **2016**, *29*, 3119–3142.



© 2017 by the authors. Licensee MDPI, Basel, Switzerland. This article is an open access article distributed under the terms and conditions of the Creative Commons Attribution (CC BY) license (<http://creativecommons.org/licenses/by/4.0/>).